Journal of Oral Biosciences 68 (2026) 100720

Contents lists available at ScienceDirect

Journal of Oral Biosciences

journal homepage: www.elsevier.com/locate/job

Dynamin 2 is involved in osteoblast migration by regulating the organization of F-actin

Takumi Moriya [a,b], A. Surong [c], Nanami Tatsumi [c], Hiroshi Yamada [c], Fumiko Takemoto [d], Hiroshi Kamioka [b], Hirohiko Okamura [a], Mika Ikegame [a,*]

[a] Department of Oral Morphology, Graduate School of Medicine, Dentistry and Pharmaceutical Sciences, Okayama University, 2-5-1, shikata-cho, Kita-ku, Okayama, 700-8525, Japan
[b] Department of Orthodontics, Graduate School of Medicine, Dentistry and Pharmaceutical Sciences, Okayama University, 2-5-1, shikata-cho, Kita-ku, Okayama, 700-8525, Japan
[c] Department of Neuroscience, Graduate School of Medicine, Dentistry and Pharmaceutical Sciences, Okayama University, 2-5-1, shikata-cho, Kita-ku, Okayama, 700-8558, Japan
[d] Department of Orthodontics, Okayama University Hospital, 2-5-1, shikata-cho, Kita-ku, Okayama, 700-8525, Japan

ARTICLE INFO

Keywords:
Dynamin
Cell migration
Osteoblasts
F-actin

ABSTRACT

Objectives: Dynamin, a GTPase that regulates membrane dynamics, has recently been implicated in actin cytoskeletal remodeling. This study aimed to elucidate the role of dynamin in osteoblast migration by examining the effects of dynamin inhibition on the localization and organization of F-actin and dynamin 2 in MC3T3-E1 cells.
Methods: MC3T3-E1 cells were treated with dynamin inhibitors (Dyngo 4a and Dynole 34-2), and cell migration was assessed using a wound-healing assay. Fluorescent staining was performed to analyze the intracellular localization of F-actin and dynamin 2.
Results: Dynamin inhibition significantly reduced the migration of MC3T3-E1 cells. Fluorescence analysis revealed a marked decrease in the accumulation and colocalization of F-actin and dynamin 2 at the protrusion edge. Additionally, dynamin inhibition suppressed the formation of lamellipodia and stress fibers while promoting the appearance of abnormal F-actin clusters in the cytoplasm.
Conclusions: These findings suggest that dynamin plays an essential role in osteoblast migration by regulating actin cytoskeletal remodeling, particularly through the formation of lamellipodia and stress fibers.

1. Introduction

Bone formation and repair are highly dynamic processes that depend on the precise regulation of osteoblast differentiation, proliferation, and migration [1,2]. Among these processes, osteoblast migration is particularly crucial during the early stages of bone formation and regeneration, as it enables cells to reach specific sites for tissue repair or growth [3]. Despite its significance, the molecular mechanisms governing osteoblast migration remain poorly understood. Cell migration fundamentally relies on the remodeling of the actin cytoskeleton, which is tightly controlled by intracellular signaling pathways and regulatory proteins [4].

Dynamin, a large GTPase traditionally known for its role in membrane fission and endocytosis, exists in three major isoforms: dynamin 1, dynamin 2, and dynamin 3 [5]. Among these, dynamin 2 is ubiquitously expressed in various tissues and is reported to be the predominant isoform in osteoblasts [6,7]. In addition to its canonical functions, dynamin has emerged as a key player in actin dynamics [8,9]. It coordinates cytoskeletal remodeling and cell motility by interacting with actin-binding proteins and modulating membrane dynamics [10,11]. Dynamin modulates the spatial distribution of membrane receptors and cytoskeletal regulators essential for directed cell movement. In particular, its interaction with cortactin via the proline-rich domain promotes actin filament organization at membrane ruffles [12], a process involving the dynamic remodeling of actin bundles and actomyosin structures [13]. Additionally, dynamin contributes to the stabilization and disassembly of actin filaments, which is critical for the formation and directional extension of cellular protrusions [11].

* Corresponding author. Department of Oral Morphology, Graduate School of Medicine, Dentistry and Pharmaceutical Sciences, Okayama University, 2-5-1, shikata-cho, Kita-ku, Okayama, 700-8525, Japan.
E-mail address: ikegame@md.okayama-u.ac.jp (M. Ikegame).

https://doi.org/10.1016/j.job.2025.100720
Received 22 July 2025; Received in revised form 25 November 2025; Accepted 27 November 2025
Available online 2 December 2025

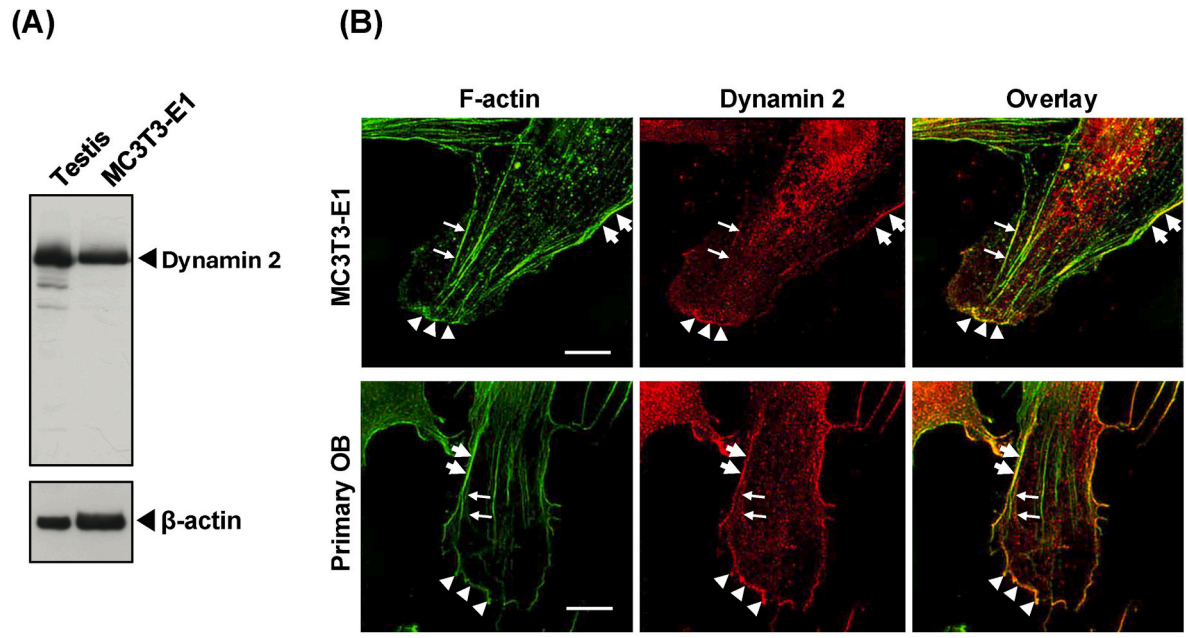

Fig. 1. Expression of dynamin 2 and subcellular distribution of dynamin 2 in osteoblasts
(A) Western blot analysis confirmed the expression of dynamin 2 in MC3T3-E1 cell lysates, using rat testis cytosolic fractions as a positive control. β-actin served as a loading control.
(B) Super-resolution images of MC3T3-E1 cells (upper panels) and primary osteoblasts isolated from chick calvariae (lower panels) stained for F-actin (green) and dynamin 2 (red). Large arrows indicate the cell cortex, arrowheads mark the lamellipodia, and small arrows highlight colocalization of F-actin and dynamin 2 in stress fibers. Scale bars: 5 μm.

Recent studies suggest that dynamin plays a crucial role in regulating osteoblast migration by facilitating directional cell movement [7]. Although previous studies have shown that inhibition of dynamin suppresses osteoblast migration, the precise subcellular mechanisms underlying this effect remain unclear. The primary aim of this study was to clarify the role of dynamin in osteoblast migration. To achieve this, we analyzed the intracellular localization of F-actin and dynamin 2, which are essential components of the cytoskeleton, to elucidate the relationship between their distribution and cell migration. Specifically, we evaluated how dynamin inhibition affects the spatial organization of these cytoskeletal elements, aiming to gain new insights into how their coordinated interaction regulates osteoblast motility. Understanding the relationship between F-actin, dynamin 2, and migration is important for establishing a foundation to uncover the molecular mechanisms that underlie osteoblast function during bone formation and regeneration.

2. Materials and methods

2.1. Cell culture

The pre-osteoblastic cell line MC3T3-E1 was purchased from the RIKEN BRC Cell Bank (Tsukuba, Japan). MC3T3-E1 cells, which are commonly used in bone research, are derived from the calvariae (skulls) of seven-day-old ddY mice. MC3T3-E1 cells were cultured in Minimum Essential Medium α (MEMα; Gibco/Life Technologies Corporation, Carlsbad, CA, USA) supplemented with 10 % Fetal Bovine Serum (Gibco/Life Technologies Limited, Paisley, Scotland, UK) and 1 % penicillin-streptomycin solution (Nacalai Tesque Inc., Kyoto, Japan) [14]. We confirmed that this cell line exhibits osteoblastic characteristics when cultured in a differentiation-inducing medium. Primary osteoblasts were isolated from 17-day-old embryonic chicken calvariae by enzymatic digestion with collagenase I (cat# SCR103; Sigma-Aldrich, St. Louis, MO, USA).

2.2. Preparation of tissue and cell proteins

To confirm the expression of dynamin 2 in osteoblasts, proteins were extracted from rat testis as a positive control and from MC3T3-E1 cells. To examine the effect of dynamin inhibitors on dynamin expression, MC3T3-E1 cells were seeded in 10-cm culture dishes (cat# 130182, Thermo Fisher Scientific, Rochester, NY, USA) at a density of 3.5×10^4 cells per dish and incubated for 48 h. The cells were then treated for 8 h with either DMSO, 5 μM Dynole 34-2 (cat# ab120463, Abcam, Cambridge, UK), or 5 μM Dyngo 4a (cat# ab120689, Abcam). After treatment, the cells were washed once with PBS (cat# 10010049, Gibco, Thermo Fisher Scientific, Waltham, MA, USA) and collected using PBS containing cOmplete, EDTA-free protease inhibitor cocktail (cat# 11697498001, Roche Diagnostics GmbH, Mannheim, Germany) with a cell scraper. Proteins were extracted according to standard procedures, and their concentrations were determined using the Bradford assay.

2.3. Western blotting

Ten micrograms of protein extracted from MC3T3-E1 cells were separated by SDS-PAGE using a 10 % polyacrylamide gel. Proteins were transferred to a PVDF membrane (cat# 10600003, Cytiva, Marlborough, MA, USA) using a wet transfer system at 100 V for 1 h at 4 °C. The membrane was blocked with 5 % skim milk (cat# 232100; BD Difco, Becton, Dickinson and Company, Sparks, MD, USA) in Tris-buffered saline containing 0.1 % Tween-20 (TBS-T) for 4 h at room temperature. After blocking, the membrane was incubated overnight at 4 °C with rabbit polyclonal anti-dynamin 2 antibody (1:1000; cat# ab65556, Abcam) and mouse monoclonal anti-β-actin antibody (1:10000; cat# A5441, Sigma-Aldrich) in blocking buffer. After five washes with TBS-T, the membranes were incubated with horseradish peroxidase-conjugated goat anti-rabbit IgG (1:2500; cat# 31460; Invitrogen, Carlsbad, CA, USA) and rabbit anti-mouse IgG (1:2500; cat# 31450; Invitrogen) for 1 h at room temperature. Following five additional washes with TBS-T, protein bands were visualized using enhanced chemiluminescence detection reagent (cat# RPN2106, Cytiva) and exposed to an X-ray film

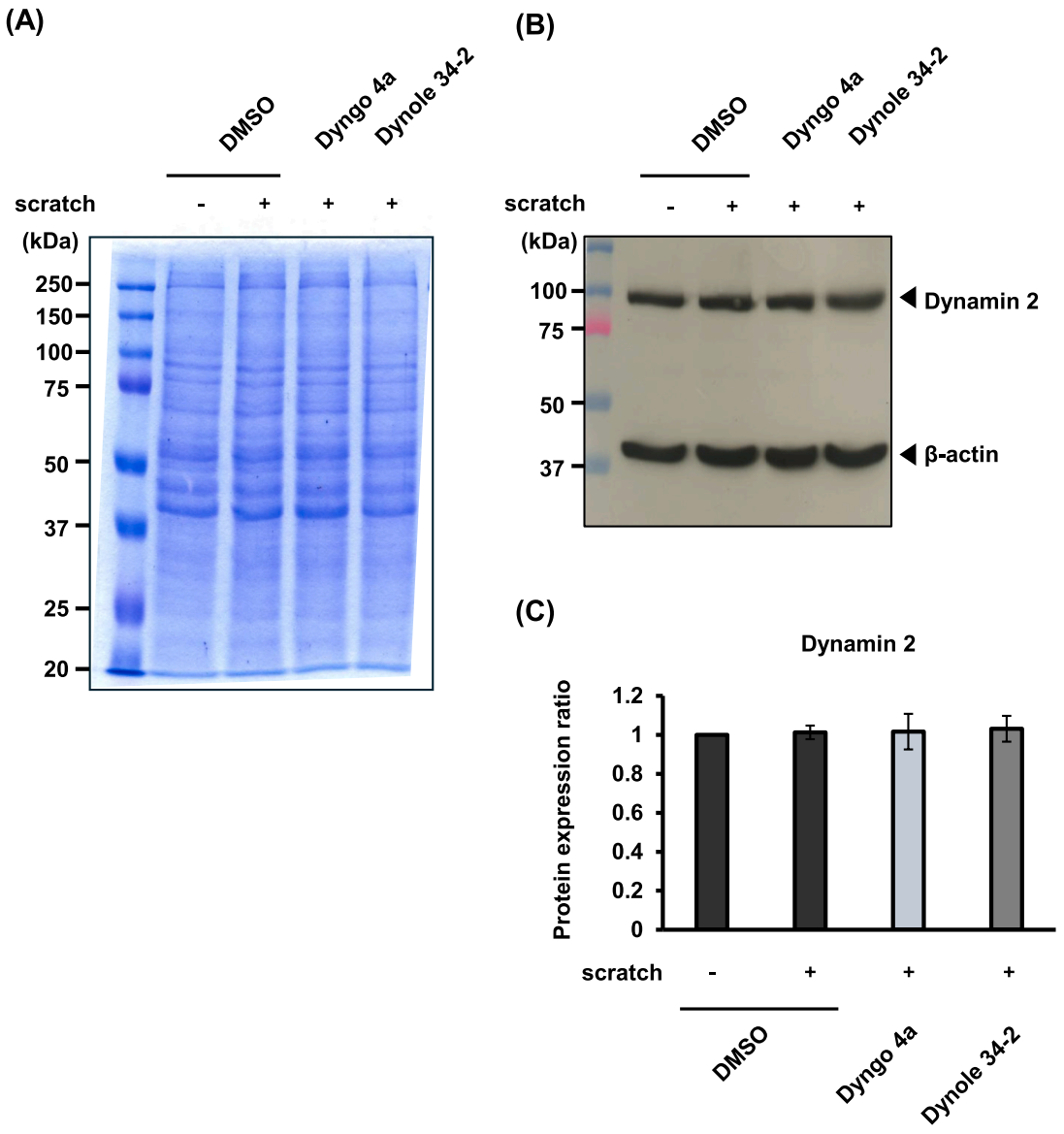

Fig. 2. The effect of dynamin inhibitors on the protein expression levels
(A) SDS-PAGE followed by Coomassie Brilliant Blue staining of total protein lysates from MC3T3-E1 cells. Control groups included unscratched cells and scratched cells treated with DMSO. Cells scratched and treated with 5 μM Dyngo 4a or 5 μM Dynole 34-2 were also analyzed after 8 h.
(B) Western blot analysis of dynamin 2 and β-actin using the same lysates. Molecular weight markers (kDa) are shown on the left.
(C) Relative protein expression levels of dynamin 2. Band intensities were quantified using ImageJ software and normalized to β-actin. The resulting values were expressed relative to the unscratched DMSO control group. No significant differences in dynamin 2 expression levels were observed among groups, indicating that neither scratch stimulation nor dynamin inhibitor treatment affected the overall protein expression levels of dynamin 2. All group comparisons showed no statistically significant differences. Data represent mean ± SEM from three independent experiments. Statistical analysis was performed using one-way ANOVA followed by Tukey's post hoc test.

(cat#2806836, Cytiva).

2.4. Wound-healing assay

The wound-healing assay was conducted as described by Liang et al. [15]. MC3T3-E1 cells were cultured in 27-mm-diameter glass-based dishes (cat# 3910-035, IWAKI, Tokyo, Japan) treated with atelocollagen (cat# IPC-50; KOKEN, Tokyo, Japan) at a density of 5×10^4 cells per dish and incubated for 24 h. Three linear scratches were created using yellow pipette tips, and the cells were washed with serum-free medium. Dynamin inhibitors were prepared in MEMα at a concentration of 5 μM and preheated at 37 °C. Cells were incubated with 2 mL of MEMα containing the inhibitor in each glass-based dish for 8 h. Images were captured using a phase-contrast microscope (IX-71; Olympus Optical Co., Ltd., Tokyo, Japan). Wound areas were measured in the phase-contrast images using ImageJ software ver. 1.53 (NIH, Bethesda, MD, USA). The scale was set based on a scale bar, and wound areas were outlined along the leading edge of the cells. The wound area was measured at 0 and 8 h, and the difference was calculated to evaluate cell migration. For each condition, measurements were performed in five randomly selected fields and quantitatively analyzed. Similar trends were observed in four independent experiments.

2.5. Immunofluorescence and fluorescent staining

MC3T3-E1 cells cultured on glass-based dishes (IWAKI) were fixed with 4 % paraformaldehyde in PBS for 15 min at room temperature, permeabilized with 0.1 % Triton X-100 (cat# X100, Sigma-Aldrich) for

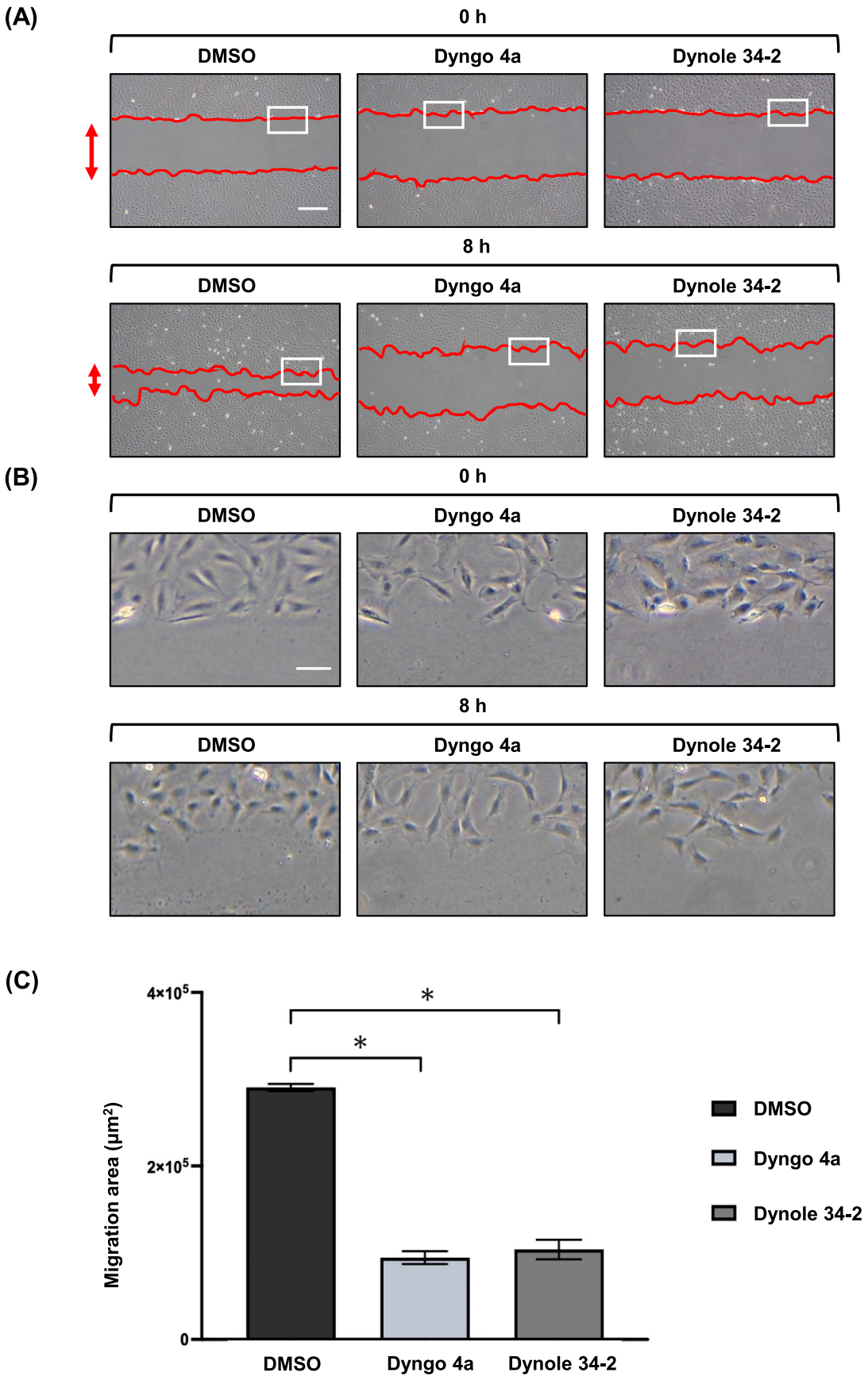

(caption on next page)

Fig. 3. Dynamin inhibition decreased migration area in a wound-healing assay
(A) Phase-contrast images showing wound areas in MC3T3-E1 cell monolayers at 0 and 8 h after scratch injury. Cells were treated with DMSO as a control, Dyngo 4a (5 μM), or Dynole 34-2 (5 μM) immediately after scratching. Red lines indicate the wound edges, and white boxes mark regions shown at higher magnification in (B). Scale bar: 100 μm.
(B) Magnified views of the white-boxed regions in (A), highlighting the morphology of migrating cells at the wound edges. Scale bar: 20 μm.
(C) Quantification of the wound area migrated for 8 h. Data are representative of one of four independent experiments in which similar inhibitory trends were observed. Migration areas were measured using ImageJ from five randomly selected fields per condition. Data represent mean ± SEM. Statistical analysis was performed using one-way ANOVA followed by Tukey's post hoc test; $^{*}p < 0.05$.

15 min, and subsequently blocked with 10 % donkey serum in PBS at 37 °C for 1 h. The cells were then incubated with rabbit polyclonal anti-dynamin 2 antibody (1:50; Abcam) at 37 °C for 2 h, followed by five washes with PBS for 5 min each. After washing, cells were incubated with Alexa Fluor 555 donkey anti-rabbit IgG (1:200; cat# A31572, Invitrogen, Carlsbad, CA, USA) and Alexa Fluor 488 phalloidin (1:40; cat# A12379, Invitrogen) for 1 h at 37 °C. After two additional washes with PBS for 5 min each, nuclei were stained with DAPI (1:1000; cat# D212, Dojindo, Kumamoto, Japan) and samples were mounted using Fluoromount (cat# k024, Diagnostic Biosystems, Pleasanton, CA, USA). Samples were examined using a spinning-disc confocal microscope system (X-Light Confocal Imager; CREST OPTICS S.P.A., Rome, Italy). The confocal system was controlled using MetaMorph software ver. 7.10.3.279 (Molecular Devices, Sunnyvale, CA, USA). A structured illumination microscope (N-SIM; Nikon, Tokyo, Japan) was used for super-resolution imaging.

2.6. Statistical analysis

All data were presented as the mean ± standard error of the mean (SEM), unless otherwise stated. Statistical analyses were performed using GraphPad Prism Software (GraphPad Software, San Diego, CA, USA). One-way analysis of variance (ANOVA), followed by Tukey's post hoc test, was used to assess differences between groups. Statistical significance was set at $p < 0.05$. All experiments were performed at least three times independently ($n \geq 3$), with triplicate samples per condition to ensure reproducibility and statistical reliability. This sample size selection follows the standard methodology commonly adopted in cell culture–based studies to minimize biological variability and provide adequate statistical power.

3. Results

3.1. Expression of dynamin 2 and subcellular distribution of dynamin 2 in osteoblasts

Although dynamin comprises three major isoforms (dynamin 1–3), dynamin 2 is ubiquitously expressed and has been reported as the predominant isoform involved in actin regulation in various cell types [16]. Therefore, we analyzed dynamin 2 in osteoblasts. Western blot analysis confirmed the expression of dynamin 2 in MC3T3-E1 cell lysates (Fig. 1A).

To determine the intracellular localization of dynamin 2, we performed immunofluorescence staining for dynamin 2 and fluorescent staining for F-actin, followed by observation using super-resolution microscopy. These observations clearly showed that dynamin 2 colocalized with F-actin at the edge of the cell cortex and lamellipodia, and partially along the stress fibers. Similar localization patterns were also observed in primary osteoblasts isolated from chick calvariae, suggesting that the characteristic distribution of dynamin 2 with actin cytoskeletal components is a common feature of osteoblasts (Fig. 1B).

3.2. Dynamin inhibitors did not change the protein expression levels of dynamin 2 and F-actin

Given the observed colocalization of F-actin and dynamin 2 in MC3T3-E1 cells, we investigated this relationship using dynamin-specific inhibitors. To examine the effect of dynamin inhibition on protein expression, MC3T3-E1 cells were scratched and treated with 5 μM of the dynamin inhibitors Dyngo 4a and Dynole 34-2 for 8 h. Proteins were extracted from each group and subjected to SDS-PAGE, followed by Coomassie Brilliant Blue (CBB) staining (Fig. 2A). CBB staining revealed no significant differences in overall band intensity among the groups, suggesting that dynamin inhibitors did not affect total protein expression levels in MC3T3-E1 cells. We then performed Western blot analysis using anti-dynamin 2 and anti-β-actin antibodies (Fig. 2B). The band intensities of both dynamin 2 and β-actin remained unchanged between the untreated and the inhibitor-treated groups (Fig. 2C).

3.3. Dynamin inhibitors suppressed MC3T3-E1 cell migration

Because dynamin inhibitors did not affect total protein levels or cell viability of MC3T3-E1 cells [Supplemental Fig. 1], we next examined whether dynamin inhibition impaired MC3T3-E1 cell migration. To this end, we performed a wound-healing assay using MC3T3-E1 cells treated with or without the dynamin inhibitors, Dyngo 4a and Dynole 34-2. The assay revealed a significant reduction in the migration area of MC3T3-E1 cells treated with either inhibitor compared with that in the control group (Fig. 3A). Phase-contrast images taken at 0 and 8 h showed no apparent morphological differences at wound edges between the groups (Fig. 3B). Wound areas at 8 h were quantified using ImageJ software (Fig. 3C), demonstrating that dynamin inhibition significantly reduced the migration area relative to control. Specifically, Dyngo 4a and Dynole 34-2 treatment resulted in a 67.5 ± 4.5 % and 64.2 ± 3.9 % decrease in migration area, respectively, compared to the control. Additional scratch assay analyses with varying inhibitor concentrations confirmed that dynamin inhibition reduced osteoblast migration, but no clear dose-dependent trend was observed within the dose range from 1 to 40 μM evaluated [Supplemental Fig. 2].

3.4. Localization of F-actin and dynamin 2 at the protrusion edge in MC3T3-E1 cells

To examine the effects of dynamin inhibition on the intracellular distribution of F-actin and dynamin 2 in osteoblasts, we performed fluorescent staining of MC3T3-E1 cells treated with dynamin inhibitors. In control cells, F-actin was observed along stress fibers, while dynamin 2 appeared as small dots distributed throughout the cell, including at the periphery (Fig. 4A). High-magnification images (Fig. 4B) revealed that both proteins accumulated at the protrusion edge, where lamellipodia were formed. In contrast, cells treated with Dyngo 4a or Dynole 34-2 showed a slight reduction in cytoplasmic stress fibers and reduced accumulation of dynamin 2 in protrusions compared to control. Moreover, lamellipodia were poorly developed, and both dynamin 2 and F-actin showed reduced localization at the protrusion edge. Additionally, relatively large F-actin clusters were more frequently observed in the protrusions of inhibitor-treated cells, showing a distinct distribution pattern from that of the control group.

4. Discussion

In this study, we investigated the role of dynamin in osteoblast migration by evaluating the localization of dynamin 2 and actin cytoskeletal structures in pre-osteoblastic MC3T3-E1 cells. We demonstrated

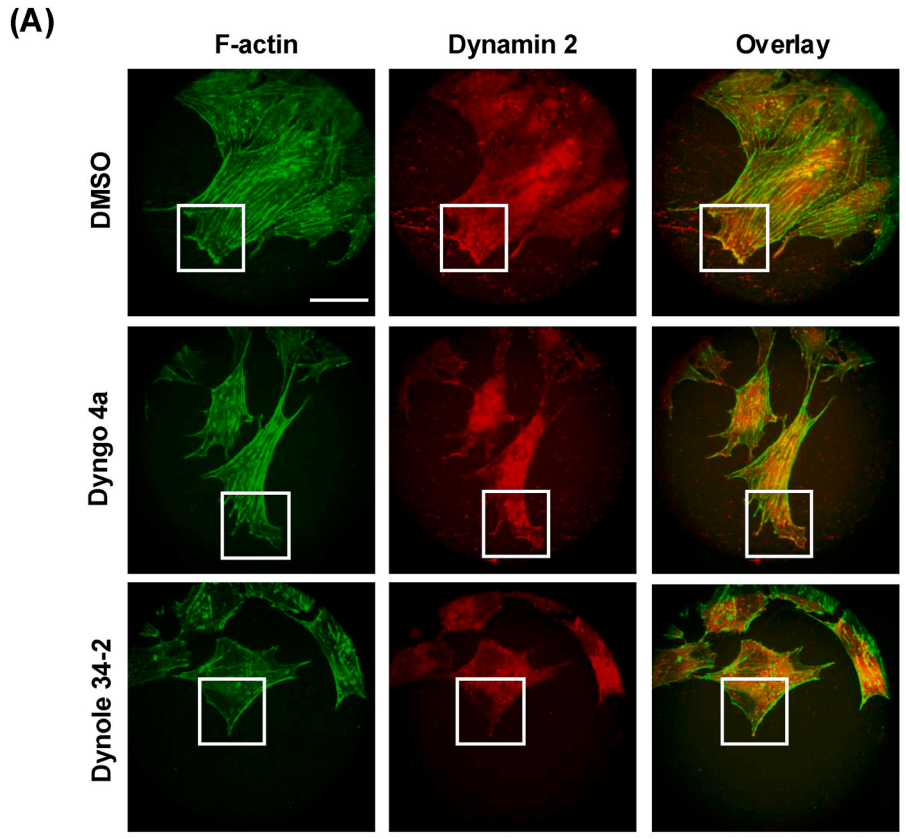

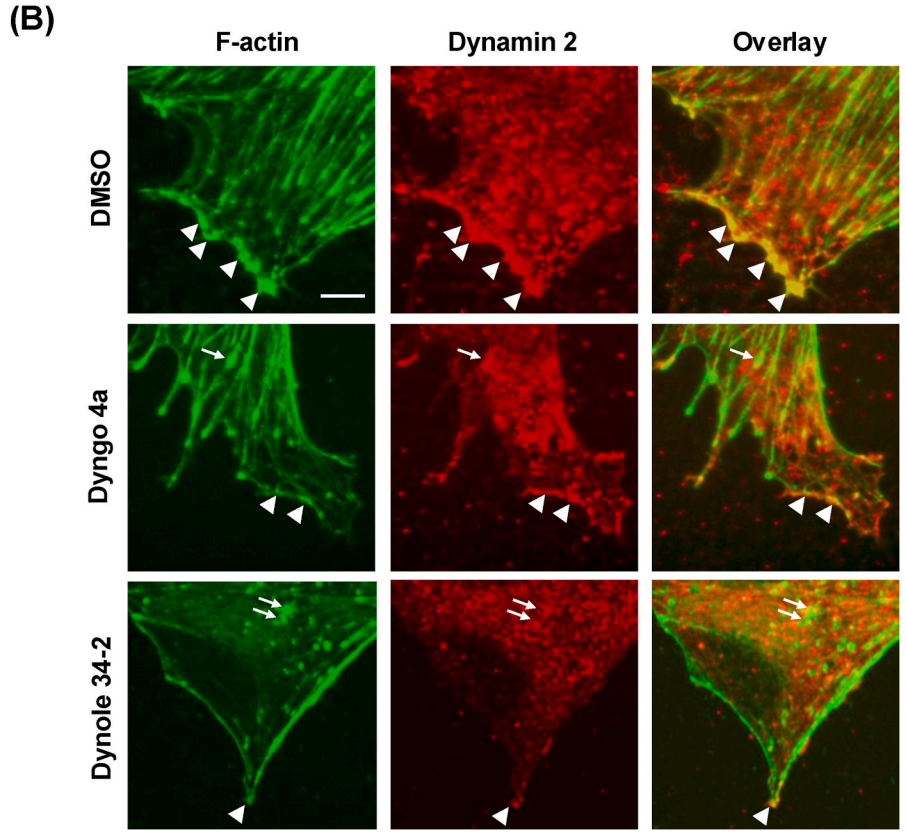

(caption on next page)

Fig. 4. Localization of F-actin and dynamin 2 at the protrusion edge in MC3T3-E1 cells
(A) Immunofluorescence images of MC3T3-E1 cells stained for F-actin (green) and dynamin 2 (red), with merged images shown on the right. White squares indicate peripheral regions of the cells facing the scratched area and are displayed at higher magnification in (B). Scale bar: 50 μm.
(B) Enlarged views of the boxed areas in (A), indicating the colocalization of F-actin and dynamin 2 at the protrusion edge (arrowheads) and F-actin clusters (small arrows) in the peripheral area. Scale bar: 10 μm.

the intracellular distribution of dynamin 2, the isoform most abundantly expressed in mesenchymal cells, including osteoblastic cells [7]. Dynamin 2 was found to colocalize with actin structures such as the cell cortex, stress fibers, and lamellipodia. This distribution pattern has been reported in various other cell types, including H1299 non-small cell lung carcinoma cells and osteosarcoma cells [11,13]. Cell migration depends on the dynamic reorganization of the actin cytoskeleton, including the formation and stabilization of protrusions, such as lamellipodia and filopodia [17]. Therefore, the localization of dynamin 2 to cell protrusions suggests its role in lamellipodia formation and cell migration in MC3T3-E1 cells.

We next examined the effects of the dynamin inhibitors Dyngo 4a and Dynole 34-2 on cell migration and the subcellular distribution of F-actin and dynamin 2 in MC3T3-E1 cells. Inhibition of dynamin activity reduced the number of actin stress fibers and the accumulation of F-actin and dynamin 2 at cell protrusions, accompanied by a marked decrease in cell migration. Dynamin stabilizes actin structures via its GTPase activity [8,11,13]. Dyngo 4a and Dynole 34-2 are small-molecule inhibitors that suppress cell migration by targeting dynamin's GTPase activity. Dyngo 4a inhibits dynamin by binding to its GTPase domain, thereby preventing vesicle scission during clathrin-mediated endocytosis [18]. In contrast, Dynole 34-2 acts through an allosteric mechanism, interfering with dynamin self-assembly and GTP hydrolysis [18–20]. Based on previous studies indicating that concentrations around 5 μM of these inhibitors are non-cytotoxic in tumor cells [11,21], we evaluated their effects in MC3T3-E1 osteoblasts. Treatment with 5 μM Dyngo 4a or Dynole 34-2 did not affect cell viability or the total protein expression levels, including those of dynamin 2 and β-actin. A previous study reported that another dynamin inhibitor, Dynasore (40 μM), suppressed the migration of murine primary osteoblasts by inhibiting dynamin GTPase activity [7]. Furthermore, hyperglycemia suppresses MC3T3-E1 cell migration and reduces dynamin 2 distribution in lamellipodia [22]. These findings suggest that the dynamin 2 GTPase activity in osteoblasts plays a crucial role in reconstructing the actin cytoskeleton to form cellular protrusions, essential for cell migration. Collectively, these findings indicate that dynamin 2 GTPase activity in osteoblasts plays a crucial role in reorganizing the actin cytoskeleton to form cellular protrusions required for migration. Consistent with these observations, a comparable inhibitory pattern was also observed in NIH3T3 fibroblast cells [Supplemental Fig. 3], suggesting that this phenomenon is not specific to osteoblasts.

Inhibition of dynamin GTPase activity also led to decreased stress fiber formation throughout the cytoplasm. In contrast, large F-actin clusters were frequently observed in the cytoplasm. Similar reductions in stress fibers and increased F-actin clustering upon dynamin inhibition have been reported previously [8,23,24], suggesting that dynamin maintains stress fibers and prevents abnormal actin aggregation by directly regulating the actin cytoskeleton. Together with our findings, these results suggest that dynamin plays an essential role in osteoblastic cells by maintaining stress fibers and preventing abnormal actin aggregation.

In addition, gene knockdown approaches, such as siRNA-mediated suppression of dynamin 2, have been shown to reduce filopodia formation in human non-small cell lung carcinoma cells [11]. Thus, similar analyses in osteoblastic cells would provide further mechanistic insights to clarify the molecular mechanisms underlying osteoblast motility.

5. Conclusion

In conclusion, this study demonstrated that inhibition of dynamin GTPase activity impairs lamellipodia and stress fiber formation, reduces dynamin 2 localization at protrusions, and suppresses cell motility in osteoblasts. These results indicate that dynamin contributes to osteoblast migration by organizing the actin cytoskeleton. Moreover, these findings provide new insights into the cellular mechanisms underlying osteoblast migration and may contribute to the development of novel therapeutic strategies aimed at enhancing bone regeneration.

Ethical approval

Ethical approval was not required for this study.

Author contribution statement

Takumi Moriya, conceptualization, methodology, investigation, validation, formal analysis, data curation, visualization, writing-original draft preparation: Surong A, methodology, investigation, validation, data curation, visualization, writing - review & editing: Nanami Tatsumi, investigation, data curation: Hiroshi Yamada, conceptualization, methodology, investigation, validation, data curation, visualization, writing-original draft preparation, resources, project administration, funding acquisition, supervision: Fumiko Takemoto, methodology, investigation, writing - review & editing, funding acquisition: Hiroshi Kamioka, investigation, writing - review & editing, resources: Hirohiko Okamura, conceptualization, methodology, investigation, validation, data curation, visualization, writing-original draft preparation, resources, project administration, funding acquisition, supervision, Mika Ikegame, conceptualization, methodology, investigation, validation, data curation, visualization, writing-original draft preparation, resources, project administration, funding acquisition, supervision.

Declaration of competing interest

The authors declare that there are no conflicts of interest.

Acknowledgements

This study was funded by a Grant-in-Aid for Scientific Research from the Ministry of Education, Science, Sports, and Culture of Japan (HO: 23K18431, 22H03511, 21K19644; MI: 22H06790; FT: 24K23553) and was also supported by JSPS Program for Forming Japan's Peak Research Universities (J-PEAKS) Grant Number JPJS00420230010.

We are grateful to all laboratory members for their valuable discussions and technical assistance, and we would also like to thank A. Sakane (Molecular and Cellular Function Unit, Institute of Photonics and Human Health Frontier, Tokushima University) and T. Kameoka (NIKON SOLUTIONS CO., LTD.) for their assistance.

Appendix A. Supplementary data

Supplementary data to this article can be found online at https://doi.org/10.1016/j.job.2025.100720.

References

[1] Rutkovskiy A, Stensløkken K-O, Vaage IJ. Osteoblast differentiation at a glance. Med Sci Monit Basic Res 2016;22:95–106.

[2] Long F. Building strong bones: molecular regulation of the osteoblast lineage. Nat Rev Mol Cell Biol 2012;13:27–38.
[3] Su P, Tian Y, Yang C, Ma X, Wang X, Pei J, et al. Mesenchymal stem cell migration during bone formation and bone diseases therapy. IJMS 2018;19:2343. https://doi.org/10.3390/ijms19082343.
[4] Tang DD, Gerlach BD. The roles and regulation of the actin cytoskeleton, intermediate filaments and microtubules in smooth muscle cell migration. Respir Res 2017;18:54. https://doi.org/10.1186/s12931-017-0544-7.
[5] Praefcke GJK, McMahon HT. The dynamin superfamily: universal membrane tubulation and fission molecules? Nat Rev Mol Cell Biol 2004;5:133–47.
[6] Cook TA, Urrutia R, McNiven MA. Identification of dynamin 2, an isoform ubiquitously expressed in rat tissues. Proc Natl Acad Sci USA 1994;91:644–8.
[7] Eleniste PP, Huang S, Wayakanon K, Largura HW, Bruzzaniti A. Osteoblast differentiation and migration are regulated by dynamin GTPase activity. Int J Biochem Cell Biol 2014;46:9–18.
[8] Gu C, Yaddanapudi S, Weins A, Osborn T, Reiser J, Pollak M, et al. Direct dynamin–actin interactions regulate the actin cytoskeleton. EMBO J 2010;29:3593–606.
[9] Taylor MJ, Lampe M, Merrifield CJ. A feedback loop between dynamin and actin recruitment during clathrin-mediated endocytosis. PLoS Biol 2012;10:e1001302. https://doi.org/10.1371/journal.pbio.1001302.
[10] Zhang R, Lee DM, Jimah JR, Gerassimov N, Yang C, Kim S, et al. Dynamin regulates the dynamics and mechanical strength of the actin wound as a multifilament actin-bundling protein. Nat Cell Biol 2020;22:674–88.
[11] Yamada H, Takeda T, Michiue H, Abe T, Takei K. Actin bundling by dynamin 2 and cortactin is implicated in cell migration by stabilizing filopodia in human non-small cell lung carcinoma cells. Int J Oncol 2016;49:877–86.
[12] McNiven MA, Kim L, Krueger EW, Orth JD, Cao H, Wong TW. Regulated interactions between dynamin and the actin-binding protein cortactin modulate cell shape. J Cell Biol 2000;151:187–98.
[13] Mooren OL, Kotova TI, Moore AJ, Schafer DA. Dynamin2 GTPase and cortactin remodel Actin filaments. J Biol Chem 2009;284:23995–4005.
[14] Kodama H, Amagai Y, Sudo H, Kasai S, Yamamoto S. Establishment of a clonal osteogenic cell line from newborn mouse calvaria. Jpn J Oral Biol 1981;23:899–901.
[15] Liang C-C, Park AY, Guan J-L. In vitro scratch assay: a convenient and inexpensive method for analysis of cell migration in vitro. Nat Protoc 2007;2:329–33.
[16] Ferguson SM, De Camilli P. Dynamin, a membrane-remodelling GTPase. Nat Rev Mol Cell Biol 2012;13:75–88.
[17] K H, Abe T, Li S-A, Masuoka Y, Isoda M, Watanabe M, et al. Dynasore, a dynamin inhibitor, suppresses lamellipodia formation and cancer cell invasion by destabilizing actin filaments. Biochem Biophys Res Commun 2009;390:1142–8.
[18] Placidi G, Mattu C, Ciardelli G, Campa CC. Small molecules targeting endocytic uptake and recycling pathways. Front Cell Dev Biol 2023;11:1125801. https://doi.org/10.3389/fcell.2023.1125801.
[19] Gordon CP, Venn-Brown B, Robertson MJ, Young KA, Chau N, Mariana A, et al. Development of second-generation indole-based dynamin GTPase inhibitors. J Med Chem 2013;56:46–59.
[20] Hill TA, Gordon CP, McGeachie AB, Venn-Brown B, Odell LR, Chau N, et al. Inhibition of dynamin mediated endocytosis by the dynoles —synthesis and functional activity of a family of indoles. J Med Chem 2009;52:3762–73.
[21] McCluskey A, Daniel JA, Hadzic G, Chau N, Clayton EL, Mariana A, et al. Building a better dynasore: the dyngo compounds potently inhibit dynamin and endocytosis. Traffic 2013;14:1272–89.
[22] Pahwa H, Khan MdT, Sharan K. Hyperglycemia impairs osteoblast cell migration and chemotaxis due to a decrease in mitochondrial biogenesis. Mol Cell Biochem 2020;469:109–18.
[23] Yamada H, Kobayashi K, Zhang Y, Takeda T, Takei K. Expression of a dynamin 2 mutant associated with Charcot-Marie-Tooth disease leads to aberrant actin dynamics and lamellipodia formation. Neurosci Lett 2016;628:179–85.
[24] Hamasaki E, Wakita N, Yasuoka H, Nagaoka H, Morita M, Takashima E, et al. The lipid-binding defective dynamin 2 mutant in Charcot-Marie-Tooth disease impairs proper actin bundling and actin organization in glomerular podocytes. Front Cell Dev Biol 2022;10:884509. https://doi.org/10.3389/fcell.2022.884509.